Biochemical and Biophysical Research Communications 682 (2023) 91–96

Contents lists available at ScienceDirect

Biochemical and Biophysical Research Communications

journal homepage: www.elsevier.com/locate/ybbrc

Crystal structure reveals canonical recognition of the phosphorylated cytoplasmic loop of human alpha7 nicotinic acetylcholine receptor by 14-3-3 protein

Nikolai N. Sluchanko [a,**], Anna A. Kapitonova [a], Mikhail A. Shulepko [b], Ilya D. Kukushkin [c,d], Dmitrii S. Kulbatskii [d], Kristina V. Tugaeva [a], Larisa A. Varfolomeeva [a], Mikhail E. Minyaev [e], Konstantin M. Boyko [a], Vladimir O. Popov [a,f], Mikhail P. Kirpichnikov [d,f], Ekaterina N. Lyukmanova [b,c,d,f,*]

[a] A.N. Bach Institute of Biochemistry, Federal Research Center of Biotechnology of the Russian Academy of Sciences, Moscow, 119071, Russia
[b] Faculty of Biology, MSU-BIT Shenzhen University, Shenzhen, 518172, China
[c] Phystech School of Biological and Medical Physics, Moscow Institute of Physics and Technology, Institutskiy per. 9, Dolgoprudny, Moscow region, 141701, Russia
[d] Shemyakin-Ovchinnikov Institute of Bioorganic Chemistry of the Russian Academy of Sciences, Moscow, 117997, Russia
[e] N.D. Zelinsky Institute of Organic Chemistry, Russian Academy of Sciences, Moscow, Russia
[f] Interdisciplinary Scientific and Educational School of Moscow University "Molecular Technologies of the Living Systems and Synthetic Biology", Biological Faculty, Lomonosov Moscow State University, Leninskie Gory, Moscow, 119234, Russia

ARTICLE INFO

Keywords:
Intracellular loop
Phosphorylation
Domain-motif interaction
Neuronal receptors
Signaling

ABSTRACT

Nicotinic acetylcholine receptors (nAChRs) are ligand-gated ion channels composed of five homologous subunits. The homopentameric α7-nAChR, abundantly expressed in the brain, is involved in the regulation of the neuronal plasticity and memory and undergoes phosphorylation by protein kinase A (PKA). Here, we extracted native α7-nAChR from murine brain, validated its assembly by cryo-EM and showed that phosphorylation by PKA *in vitro* enables its interaction with the abundant human brain protein 14-3-3ζ. Bioinformatic analysis narrowed the putative 14-3-3-binding site down to the fragment of the intracellular loop (ICL) containing Ser365 (Q^{361}RRCSLASVEMS^{372}), known to be phosphorylated *in vivo*. We reconstructed the 14-3-3ζ/ICL peptide complex and determined its structure by X-ray crystallography, which confirmed the Ser365 phosphorylation-dependent canonical recognition of the ICL by 14-3-3. A common mechanism of nAChRs' regulation by ICL phosphorylation and 14-3-3 binding that potentially affects nAChR activity, stoichiometry, and surface expression is suggested.

1. Introduction

Nicotinic acetylcholine receptors (nAChRs) are pentameric ligand-gated ion channels. Human neuronal nAChRs are distributed in different brain areas and non-neuronal tissues [1]. The homopentameric α7-nAChR is involved in the regulation of neuronal plasticity and memory [2]. Dysfunctions of α7-nAChR provoke neuropathologies and cancer progression [3,4].

Proper folding and trafficking of α7-nAChR depend on the interaction with NACHO [5] and RIC3 [6], while modulation of α7-nAChR function is determined by endogenous acetylcholine and Ly-6 proteins [7]. Each α7-nAChR subunit consists of an extracellular domain (ECD), transmembrane domain (TM), and intracellular domain containing two α-helices and prolonged disordered intracellular loop (ICL [8,9]) responsible for the interaction with G proteins [10], Janus Kinase 2 [11], and PI3K [12]. ICL is phosphorylated by protein kinase A (PKA) [9,13], although the mechanistic consequences of this remain unclear.

The cytosolic dimeric 14-3-3 proteins recognize phosphorylated

Abbreviations: ECD, extracellular domain; ICL, intracellular loop; nAChR, nicotinic acetylcholine receptor; PKA, protein kinase A; SEC, size-exclusion chromatography; SMALP, styrene–maleic acid lipid particles; TM, transmembrane domain; TRX, thioredoxin.

* Corresponding author. Faculty of Biology, MSU-BIT Shenzhen University, Shenzhen, 518172, China.
** Corresponding author.
E-mail addresses: nikolai.sluchanko@mail.ru (N.N. Sluchanko), lyukmanova_ekaterina@smbu.edu.cn (E.N. Lyukmanova).

https://doi.org/10.1016/j.bbrc.2023.09.086
Received 21 September 2023; Accepted 27 September 2023
Available online 28 September 2023

serine/threonine residues in distinct molecular contexts, such as RX_{2-3}(pS/pT)X(P/G) [14]. There are seven 14-3-3 isoforms in humans, named by the Greek letters β, γ, ε, ζ, η, σ, τ; each monomer contains a conserved groove for phosphopeptide fragment recognition [15]. Isoforms of 14-3-3 are often interchangeable in binding a given phosphopeptide, differing by affinities but not the overall binding mode [16]. Phosphorylated disordered regions are preferred by 14-3-3 [17] and their wide occurrence in kinases and phosphatases, cytoskeletal proteins, pro- and anti-apoptotic proteins, ion channels, and membrane receptors makes 14-3-3 proteins key physiological regulators [18].

NACHO and 14-3-3η were reported to regulate the subunit stoichiometry of α4β2-nAChR [19]. Interaction of 14-3-3η with α4 nAChR subunit is mediated by a $RSLS^{467}VQ$ sequence (hereinafter, numbering is given for full nAChR sequences including signal peptides) recognized by PKA [20]. 14-3-3 binding at another motif within ICL of the α3 nAChR subunit links this receptor subunit to a multiprotein complex essential for targeting of α3-containing nAChRs to synapses [21]. In insects, another PKA-phosphorylatable 14-3-3-binding motif, $RSPS^{337}TH$, within ICL of α8-nAChR subunits was identified [22]. Therefore, 14-3-3 proteins are likely to participate in various nAChR-related processes, which are still incompletely understood.

Here, we discovered the 14-3-3 interaction with native neuronal α7-nAChR phosphorylated by PKA *in vitro* and revealed the 14-3-3 protein/ICL peptide interface by X-ray crystallography, confirming the important role of $RRCS^{365}LA$ motif phosphorylation.

2. Materials and methods

2.1. Bacterial expression of TRX-Strep-LT fusion protein

To extract native α7-nAChR from the mouse brain homogenate, we used recombinant chimeric neurotoxin LT, an efficient inhibitor of this receptor [23], produced in *E. coli* cells. For further purification of the α7-nAChR/LT complex, we used Strep-tag linked to the toxin molecule. LT contains five disulfide bonds, and addition of Strep-tag could influence the toxin folding, thus we produced LT as a fusion protein with thioredoxin (TRX). Such fusion construct previously was used for successful production of homologous neurotoxin NTII [24]. TRX and LT molecules were fused by a linker containing Strep-tag and the site for cleavage by thrombin (Fig. 1A). Production of TRX-Strep-LT was as described in Ref. [24] except the use of Origami 2(DE3) cells. TRX-Strep-LT was purified using Strep-Tactin XT Sepharose (Cytiva). TRX-Strep-LT was eluted by 50 mM biotin (Sigma) and dialyzed against TBS buffer.

2.2. Electrophysiological recordings in X. laevis oocytes

To confirm TRX-Strep-LT activity, we used two-electrode voltage clamp recordings in *Xenopus laevis* oocytes expressing human α7-nAChR as described in Ref. [23].

2.3. Animals

Animal care and experimental procedures were performed in accordance with the guidelines of EU Directive 2010/63/EU for animal experiments and approved by the Ethical Committee of the Shemyakin-Ovchinnikov Institute of Bioorganic Chemistry RAS for the control of the maintenance and use of animals (protocol #222 from February 13, 2018). Male mice at the age of 8 months were anesthetized with 2% vaporized isoflurane and sacrificed by cervical dislocation. Whole mice brains were immediately isolated, frozen in liquid nitrogen and stored at −80 °C before the experiment.

2.4. Reconstitution of the α7-nAChR/LT/14-3-3ζ complex

Whole murine brains were homogenized (60 mg of brains in 1 ml of TBS buffer supplemented with protease inhibitor cocktail: 1 mM PMSF, 0.8 μM aprotinin, 4.3 μM leupeptin, 2 μM pepstatin A (Sigma), and SMALP 140 (Cube-biotech) was added up to 2.5%. Suspension was solubilized overnight at 4 °C under stirring and clarified by centrifugation for 1 h at 100,000 g, 4 °C. TRX-Strep-LT was added up to 0.3 mg/ml to the supernatant containing extracted α7-nAChRs/SMALP, and the mixture was incubated for 8 h at 4 °C under stirring. α7-nAChR/TRX-Strep-LT complex was immobilized on the Strep-Tactin XT Sepharose

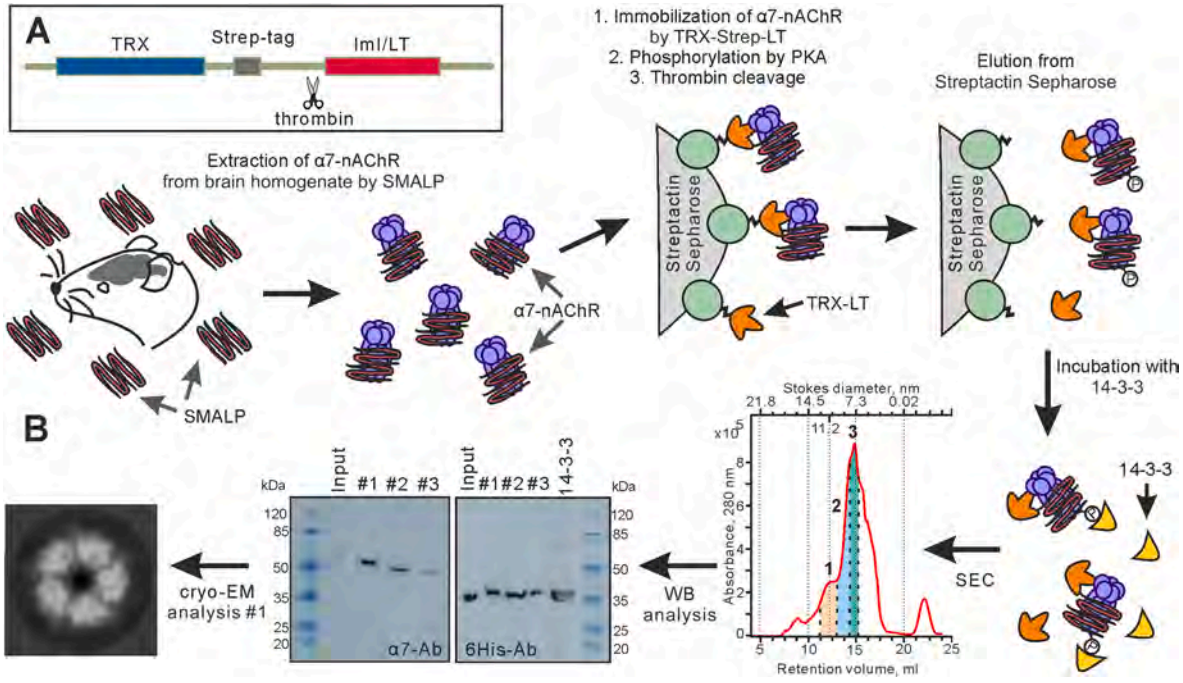

Fig. 1. Interaction of 14-3-3ζ with native α7-nAChR extracted from murine brain homogenate by TRX-Strep-LT. (A). Design of the fusion proteins consisted of TRX and the neurotoxins ImI or LT. (B). Workflow and results of Western blotting and cryo-EM analyses (example of 2D classes, size of the mask 20 nm) of α7-nAChR/SMALP extracted from murine brain homogenate by TRX-Strep-LT. Whole western blot membranes are shown in Fig. S2.

resin by overnight incubation at 4 °C under mild stirring. The resulting resin was transferred to a gravity flow column and washed with 10 V of phosphorylation buffer (12.5 mM Hepes, 1 mM $MgCl_2$, 2.5 mM NaCl, pH 7.3). Phosphorylation of immobilized α7-nAChR was carried out by incubation with 0.075 mM ATP and 0.025 mg/ml His_6-tagged catalytic subunit of mouse PKA [25] for 1 h at 37 °C. The resin was washed with 3 V of TBS followed by incubation with thrombin (20 u/mg of fusion protein, Technologia Standart) for 4 h, 4 °C. Sample eluted from the resin after thrombin cleavage was incubated with 1.3 mg/ml His_6--tagged recombinant 14-3-3ζ [25] for 1 h, 4 °C and then concentrated using a 100-kDa cut-off centricon (Millipore). Purification of the α7-nAChR/LT/14-3-3ζ complex was carried out by size-exclusion chromatography (SEC) on a Superdex 200 Increase 10/300 column (Cytiva) calibrated by thyroglobulin (17 nm), ferritin (12.2 nm), aldolase (9.6 nm), BSA (7.1 nm), and ovalbumin (6.1 nm). Chromatographic fractions were concentrated and analyzed by Western blotting and cryo-EM.

2.5. Western blotting

Detection of the complex α7-nAChR/(His_6-tagged 14-3-3ζ) in SEC fractions was carried out by Western blotting using primary Abs ABIN5611363 (1:1000, Antibodies Online), and secondary Abs 111-035-003 (1:5000, Jackson Immunoresearch) for α7-nAChR; and HRP-conjugated anti His-Tag Abs (A7058, 1:5000, Sigma) for 14-3-3ζ.

2.6. Cryo-EM sample preparation and image collection

Grids preparation, particle picking, and images collection and analysis were performed as described in Ref. [26].

2.7. Cloning, expression, and purification of 14-3-3ζ-α7(ICL)^{365} chimera

The gene encoding the chimeric protein composed of human 14-3-3ζ (Uniprot ID P63104, residues M^1-T^{229}, optimized for PKA co-expression and crystallization [16,25]) and the functional ICL fragment of human α7-nAChR (Uniprot ID: P36544, residues Q^{361}RRCSLASVEMS^{372}, α7(ICL)^{365}) connected by the GGGG linker to the *C*-terminus of 14-3-3ζ, was obtained by replacement of the gene encoding NPM1 peptide in the gene construction for another 14-3-3ζ chimera [25] by the α7(ICL)^{365} sequence.

The DNA insert was obtained in one-step PCR using T7 forward primer and the 1433za7_365 reverse primer 5′-TATATCTCGAGTCACGACATTTCTACTGAAGCCAAAGAGCAACGACGTTGACCACCTCCACCGGTC-3′, and cloned into the *pET28-His-3C* vector using *Nde*I and *Xho*I sites.

Expression, phosphorylation, and purification of the chimera were performed as described earlier [25].

2.8. Thermal shift assay

Unphosphorylated or phosphorylated chimera (40 μl, final protein concentration 4 μM) were supplemented with ProteOrange (Lumiprobe; final concentration 5X) and subjected to thermal unfolding profiling as described earlier [25].

2.9. Protein crystallization

Crystallization screening of the 14-3-3ζ-α7(ICL)^{365} chimera (24 mg/ml in 20 mM Tris-HCl buffer, pH 7.6, 150 mM NaCl) was performed as described in Ref. [25]. Best crystals grew at 15 °C in 0.2 M magnesium acetate tetrahydrate, 0.1 M sodium cacodylate trihydrate pH 6.5, 20% PEG 8000, were cryoprotected by 20% ethylene glycol (Hampton Research, USA) and flash-frozen in liquid nitrogen.

2.10. X-ray data collection and structure determination

Diffraction data were collected at 100 K at a Rigaku OD XtaLAB Synergy-S diffractometer (Rigaku, USA) and processed in CrysAlisPro software (Oxford Diffraction/Agilent Technologies UK Ltd, Yarnton) (Table S1). The structure was solved by MOLREP [27] using 14-3-3ζ structure (PDB ID: 6FNC) as a search model. Linker and phosphopeptide residues were build based on the difference electron density maps *de novo* in COOT [29]. The refinement was carried out using REFMAC5 [28] involving hydrogens in riding positions, isotropic individual atom B-factors as well as NCS and TLS (Table S1).

3. Results and discussion

3.1. Recombinant 14-3-3ζ interacts with native human α7-nAChR phosphorylated by PKA

Phosphorylation of α7-nAChR's ICL by PKA modulates the function of this receptor and its surface expression [13]. Given that 14-3-3 proteins often recognize PKA-phosphorylated motifs in their targets [30], we suggested the direct interaction between 14-3-3 and PKA-phosphorylated α7-nAChR.

To test this, we first extracted the native receptor from murine brain homogenate using recombinant analogs of selective α7-nAChR inhibitors as the baits: α-conotoxin ImI from *Conus imperialis* [31] and three-finger neurotoxin LT, a homolog of NTI from *Naja oxiana* [23]. Both neurotoxins were expressed as fusion proteins with TRX containing Strep-tag for specific isolation of the α7-nAChR/neurotoxin complex. The linker between TRX and neurotoxins' molecules contained the site for thrombin cleavage (Fig. 1A). Electrophysiological study of the fusion proteins in *Xenopus laevis* oocytes expressing α7-nAChR revealed that only TRX-Strep-LT demonstrated irreversible inhibitory activity at the receptor (IC_{50} ~ 1 μM, Figs. S1A and B), while TRX-Strep-ImI showed significantly lower activity and reversible binding to the receptor (Fig. S1A). Notably, LT inhibits α7-nAChR with nanomolar activity [23]. Given the preservation of the correct spatial structure of LT within the fusion as confirmed by NMR (Fig. S1C), a diminished activity of TRX-Strep-LT was likely caused by fused TRX. Nevertheless, the LT interaction with α7-nAChR was irreversible (Fig. 1SA), and for further work TRX-Strep-LT was chosen.

To solubilize α7-nAChR from the brain homogenate and stabilize it in solution, we used styrene maleic anhydride polymers (SMALP) forming lipodiscs with the incorporated receptor [32]. SMALP-treated, clarified brain homogenate was incubated with TRX-Strep-LT and then loaded on Strep-Tactin Sepharose to extract the α7-nAChR/LT complexes (Fig. 1B). Immobilized via LT, the receptor was phosphorylated *in vitro* by PKA directly on the resin, washed, and then detached from the resin by thrombin treatment. Eluted α7-nAChR/LT complexes were incubated with recombinant *N*-terminally His_6-tagged 14-3-3ζ and then purified by SEC. Western blotting revealed that the SEC fraction#1 corresponding to large particles with an average diameter of ~11 nm demonstrated the highest α7-nAChR content and contained 14-3-3ζ (Fig. 1B). Keeping in mind a lower size of a 14-3-3ζ dimer (~7 nm), we assumed the α7-nAChR/14-3-3ζ complex formation in the fraction#1, while the fraction#3 contained 14-3-3ζ excess (Fig. 1B). Cryo-EM analysis of the fraction#1 confirmed the native pentameric organization of α7-nAChR in the complex with LT and 14-3-3ζ, although the collected dataset did not allow us to observe the side projections of the complex and to unequivocally determine the 14-3-3-binding site(s).

3.2. ICL of α7-nAChR contains a putative 14-3-3-binding site phosphorylated by PKA

To evaluate putative 14-3-3-binding sites in human α7-nAChR (Fig. 2A), state-of-the-art tools 14-3-3-Pred (http://www.compbio.dundee.ac.uk/1433pred), 14-3-3-site finder (https://rconnect.byu.edu/

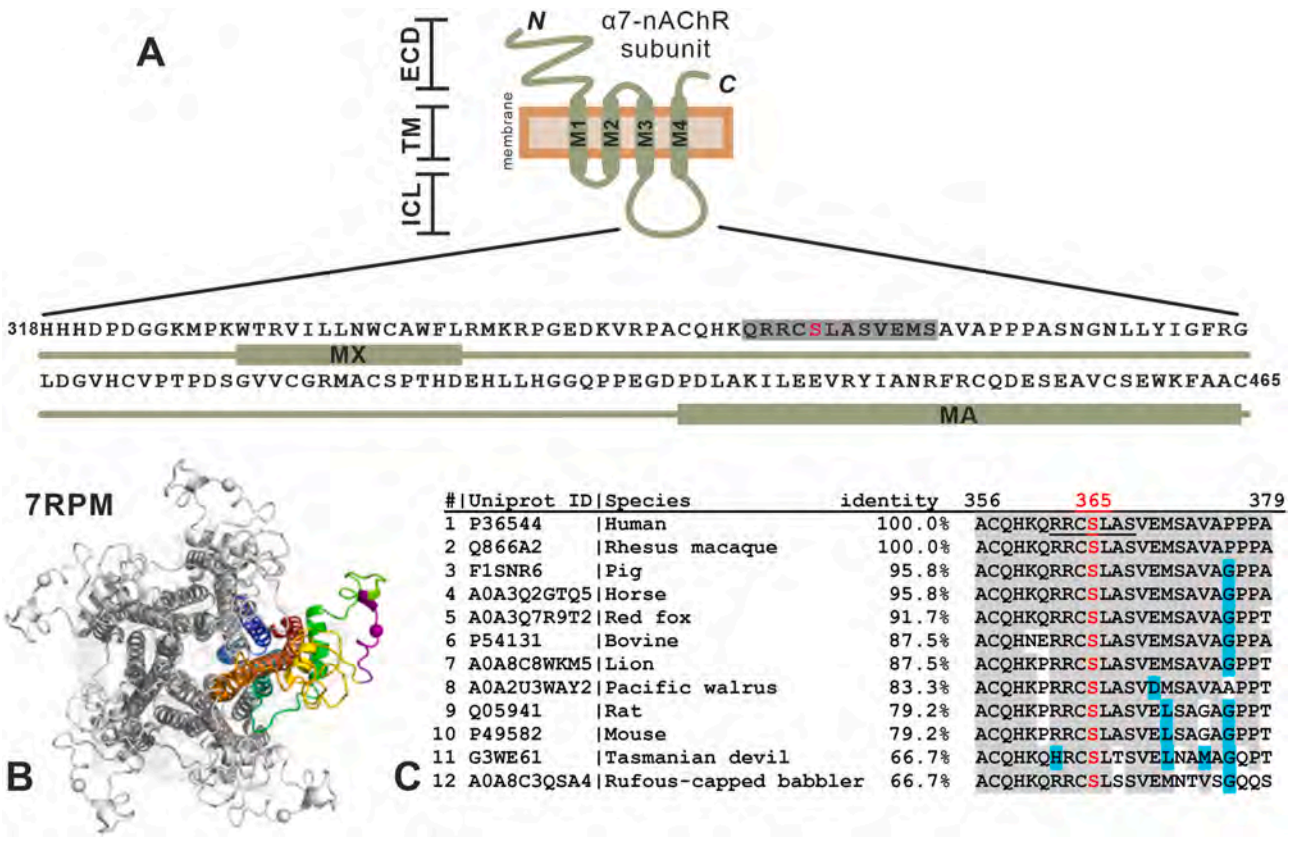

Fig. 2. Conserved Ser365-containing motif in vertebrate α7-nAChRs. (A). Sequence of the intracellular loop (ICL) of α7-nAChR. The putative 14-3-3-binding site is shown by gray. Ser365 residue phosphorylated by PKA is in red. MA and MX are helices according to Uniprot ID: P36544. (B). Structure of human α7-nAChR (PDB ID 7RPM) showing the location of the Ser365-containing motif (magenta, top view). (C). PKA-phosphorylatable site within ICL in various α7-nAChR orthologs. Identical residues are highlighted by gray, similar residues are highlighted by cyan according to five similarity groups: D,E/W,Y,F/R,K,H/N,Q/M,V,I,L,A/G,C,P,S,T. Notably, numbers are given for the full α7-nAChR sequence with signal peptide. (For interpretation of the references to color in this figure legend, the reader is referred to the Web version of this article.)

14-3-3-site-finder/), and PhosphoSitePlus (https://www.phosphosite.org/homeAction.action) were used. Among ten sites in full-length α7-nAChR considered, only four sites are known to be phosphorylated *in vivo* (T83, T221, T225, S365). Among three predicted 14-3-3-binding sites with scores above 0.5 (T230, S289, and S365), S365 has the highest scores and is the only known to be phosphorylated (Table 1). It is located within ICL (Fig. 2A and B) and is conserved in vertebrates (Fig. 2C). Being important for phosphorylation by PKA and for α7-nAChR function [13], it is likely recognized by 14-3-3, which required straight testing.

Table 1
Potential 14-3-3-binding sites in human α7-nAChR.

Site	Context sequence (phosphoS/T in square brackets)	PhosphoSitePlus annotated	14-3-3-Pred consensus score	14-3-3 site finder, top 10% (rank)
T83	WLQMSW **[T]** DHYL	+	**0.324**	-
S92	YLQWNV **[S]** EYPG	-	**0.267**	-
S117	DILLYN **[S]** ADER	-	**0.106**	+ **(5th)**
T125	DERFDA **[T]** FHTN	-	**0.213**	+ **(4th)**
T221	EPYPDV **[T]** FTVT	+	**−0.243**	-
T225	DVTFTV **[T]** MRRR	+	**−0.144**	-
T230	VTMRRR **[T]** LYYG	-	**0.789**	++ **(3rd)**
S289	MPATSD **[S]** VPLI	-	**0.714**	++ **(2nd)**
S365	HKQRRC **[S]** LASV	+	**0.992**	+++ **(1st)**
S413	CGRMAC **[S]** PTHD	-	**0.046**	+ **(6th)**

3.3. *Structural interface between 14-3-3ζ and phosphorylated α7(ICL)^{365}*

Protein-peptide approach is widely adopted for 14-3-3 proteins as they preferentially recognize flexible regions in their partners [17]. To this end, 14-3-3-peptide chimeras, in which the partner peptide fragment is phosphorylated by co-expressed PKA in *E. coli*, are particularly useful [25]. Therefore, we fused the ICL peptide Q^{361}RRC**S**^{365}LASVEMS^{372} from human α7-nAChR (α7(ICL)^{365}), which includes the minimal predicted 14-3-3-binding site RRCS^{365}LA (Table 1), to the *C*-terminus of human 14-3-3ζ and expressed the chimera with or without the constitutively active PKA.

PKA co-expression led to the downward shift on native PAGE, indicating stoichiometric chimera phosphorylation (Fig. 3A). This increased thermal stability of the chimera (Fig. 3B), indicating the formation of the 14-3-3/phosphopeptide complex [25]. Importantly, no 14-3-3ζ/α7(ICL)^{365} interaction was observed without PKA phosphorylation (Fig. 3A and B), which confirmed the phosphorylation-mediated recognition and enabled structural analysis.

Crystallization of the phosphorylated 14-3-3ζ-α7(ICL)^{365} chimera allowed X-ray structure determination at 1.95 Å resolution. The asymmetric unit contained two 14-3-3ζ subunits each with Q^{361}RRC**pS**^{365}LASVEMS^{372} peptide bound in the amphipathic groove of 14-3-3ζ (Fig. 3C), like in other 14-3-3/phosphopeptide complexes [30]. The observed 14-3-3-bound conformation of the target phosphopeptide revealed the R362-S368 region of α7-nAChR involved in the interaction. It is canonically stabilized by the coordination of the Ser365's phosphate

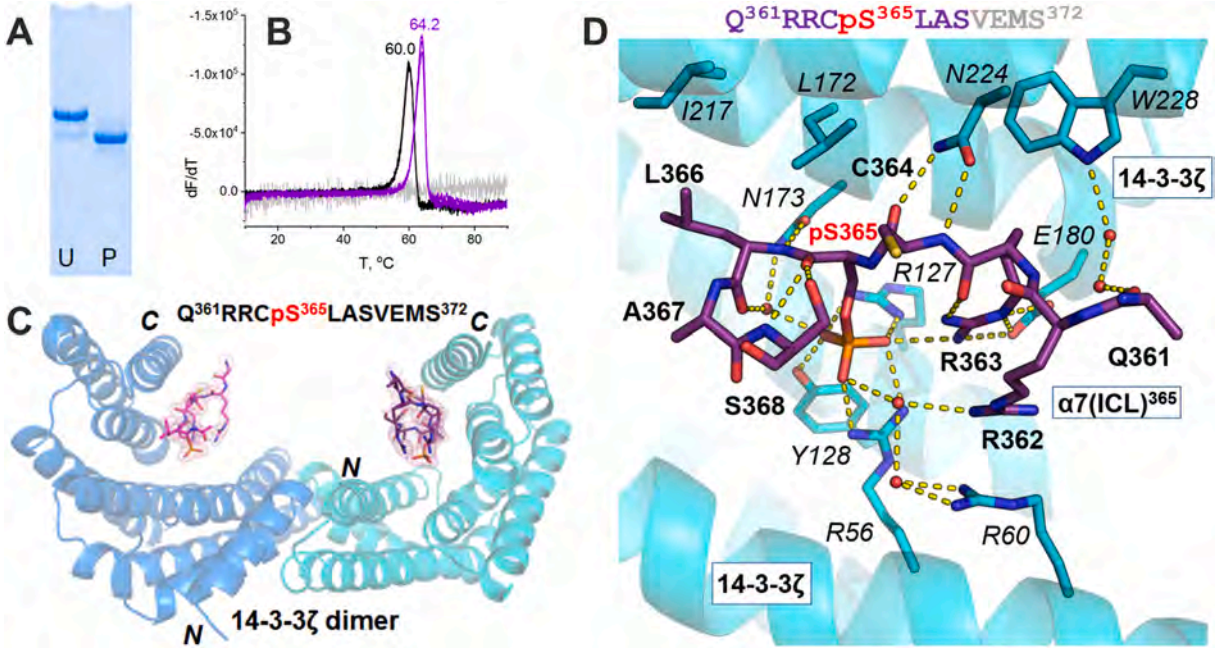

Fig. 3. Recognition of the Q^{361}RRC**pS^{365}**LASVEMS^{372} fragment of ICL of α7-nAChR by human 14-3-3ζ. (A). Native SDS-PAGE of the purified unphosphorylated (U) and phosphorylated (P) 14-3-3ζ-α7(ICL)^{365} chimera. (B). Thermal denaturation of the unphosphorylated (black trace) or phosphorylated (purple trace) chimera detected by changes of ProteOrange fluorescence intensity at a constant heating of 1 °C/min. The first derivative of the raw data is presented. The control curve for buffer is shown by light gray. T_m of the peaks is shown in °C. (C). Crystal structure of the phosphorylated 14-3-3ζ-α7(ICL)^{365} chimera showing the 14-3-3ζ dimer (tints of blue) with two copies of the Q^{361}RRC**pS^{365}**LASVEMS^{372} peptide bound in the 14-3-3 grooves. The 2Fo-Fc electron density for the peptide fragments contoured at 1σ is shown by thin mesh with the same color as the peptides themselves. Linker residues are omitted for clarity. (D). Close up view of the interface formed between the Q^{361}RRC**pS^{365}**LASVEMS^{372} peptide (violet sticks) and 14-3-3ζ (cyan). Residues of 14-3-3ζ are shown in italics. Bridging water molecules are shown by small red spheres, H-bonds are shown by yellow dashed lines. Alternative conformations of C364 and Q361, and the side chain of the latter are omitted. (For interpretation of the references to color in this figure legend, the reader is referred to the Web version of this article.)

moiety by Arg56, Arg127 and Tyr128 of 14-3-3ζ, and water-mediated contacts with Arg60 *in-trans* and Arg362 *in-cis* (Fig. 3D). Leu366 of the peptide faces the hydrophobic side of the 14-3-3 groove, in line with the known preference toward hydrophobic aliphatic side chains in this position [14]. Asn173 and Asn224 of 14-3-3ζ contribute to the canonical stabilization of the peptide backbone conformation [30]. Ser368 of the peptide contacts the backbone carbonyl of pSer365, stabilizing a *C*-terminal kink of the peptide chain (Fig. 3D), reminiscent of several other 14-3-3 complex structures in leaving the fusicoccin-binding cleft for possible modulation by drugs [33].

The observed phosphopeptide conformation indicates that the recognition of the Q^{361}RRC**pS^{365}**LASVEMS^{372} fragment of ICL of human α7-nAChR by 14-3-3ζ is highly similar to other 14-3-3/phosphopeptide complexes [30], hinting at the fundamental role of 14-3-3ζ binding to α7-nAChR. PKA phosphorylation of Ser365 in α7-nAChR is known to downregulate this receptor [13]. 14-3-3 proteins are highly abundant in the human brain reaching >1% of soluble neuronal proteins (https://pax-db.org) and are, therefore, well expected partners of α7-nAChR in this tissue. We propose either a direct modulatory effect of S365 phosphorylation and 14-3-3 binding on the α7-nAChR activity via ICL stabilization in a distinct conformation with restricted dynamics, or an indirect effect of such binding on the surface expression of α7-nAChR, for example, via masking the endoplasmic retention dibasic motifs, like for other membrane proteins [34].

Conserved in α7-nAChR orthologs, the S365 site may be absent in other nAChR subunits. Yet, the presence of alternative sites for PKA phosphorylation and 14-3-3 binding (e.g., S467 in rat α4 [20] and Ser337 in insect α8 [22]) suggests the common mechanism of regulation of different nAChRs by ICL phosphorylation and 14-3-3 binding. Another potential mechanism can exploit 14-3-3 binding to modulate the nAChRs assembly mediated by ICL recognition. By having distinct binding sites on ICLs of various nAChR subunits, 14-3-3 dimers could regulate nAChRs stoichiometry, favoring the assemblies with matching combinations of binding site pairs; that requires further investigations.

In summary, to the best of our knowledge, this is the first structure of the intracellular loop from any nAChR in complex with a partner protein. High resolution achieved (1.95 Å) enables consideration of the obtained complex as a new drug target [33]. Furthermore, our data provide insights into the potential commonality of the regulatory mechanism based on the ICL phosphorylation and 14-3-3 binding for various nAChR types, which probably deals with constraining the intrinsic dynamics of this physiologically relevant structural element.

Author contributions

A.A.K., K.V.T., I.D.K., M.A.S., and N.N.S. produced and purified proteins; D.S.K. performed electrophysiological studies; L.A.V. crystallized proteins; K.M.B. harvested crystals, collected diffraction data and helped with structure determination/refinement; N.N.S. K.M.B., M.A.S., and E.N.L. analyzed data; N.N.S. solved structure; N.N.S., E.N.L., and M.A.S. wrote the paper with input from all authors; V.O.P. and M.P.K. funding acquisition.

Data availability

Atomic coordinates and structure factors have been deposited to the Protein Data Bank under the accession code 8P1H.

Declaration of competing interest

The authors declare that they have no known competing financial interests or personal relationships that could have appeared to influence the work reported in this paper.

Acknowledgements

The study was supported by the Ministry of Science and Higher education of the Russian Federation in the framework of the Agreement no. 075-15-2021-1354 (07.10.2021). Expression and purification of 14-3-3 were partially supported by the Russian Science Foundation (no. 19-74-10031). We are grateful for Yu. Chesnokov from the Research Center "Kurchatov Institute" for assistance with cryo-EM data collection.

Appendix A. Supplementary data

Supplementary data to this article can be found online at https://doi.org/10.1016/j.bbrc.2023.09.086.

References

[1] M. Zoli, S. Pucci, A. Vilella, C. Gotti, Neuronal and extraneuronal nicotinic acetylcholine receptors, Curr. Neuropharmacol. 16 (2018) 338–349, https://doi.org/10.2174/1570159X15666170912110450.
[2] F. Koukouli, J.-P. Changeux, Do nicotinic receptors modulate high-order cognitive processing? Trends Neurosci. 43 (2020) 550–564, https://doi.org/10.1016/j.tins.2020.06.001.
[3] A.V. Terry, K. Jones, D. Bertrand, Nicotinic acetylcholine receptors in neurological and psychiatric diseases, Pharmacol. Res. 191 (2023), 106764, https://doi.org/10.1016/j.phrs.2023.106764.
[4] J.R. Friedman, S.D. Richbart, J.C. Merritt, K.C. Brown, N.A. Nolan, A.T. Akers, J. K. Lau, Z.R. Robateau, S.L. Miles, P. Dasgupta, Acetylcholine signaling system in progression of lung cancers, Pharmacol. Ther. 194 (2019) 222–254, https://doi.org/10.1016/j.pharmthera.2018.10.002.
[5] S. Gu, J.A. Matta, B. Lord, A.W. Harrington, S.W. Sutton, W.B. Davini, D.S. Bredt, Brain alpha 7 nicotinic acetylcholine receptor assembly requires NACHO, Neuron 89 (2016) 948–955, https://doi.org/10.1016/j.neuron.2016.01.018.
[6] M.E. Williams, B. Burton, A. Urrutia, A. Shcherbatko, L.E. Chavez-Noriega, C. J. Cohen, J. Aiyar, Ric-3 promotes functional expression of the nicotinic acetylcholine receptor alpha 7 subunit in mammalian cells, J. Biol. Chem. 280 (2005) 1257–1263, https://doi.org/10.1074/jbc.M410039200.
[7] J.M. Miwa, K.R. Anderson, K.M. Hoffman, Lynx prototoxins: roles of endogenous mammalian neurotoxin-like proteins in modulating nicotinic acetylcholine receptor function to influence complex biological processes, Front. Pharmacol. (2019) 10. https://www.frontiersin.org/articles/10.3389/fphar.2019.00343. (Accessed 2 September 2023).
[8] V. Bondarenko, M.M. Wells, Q. Chen, T.S. Tillman, K. Singewald, M.J. Lawless, J. Caporoso, N. Brandon, J.A. Coleman, S. Saxena, E. Lindahl, Y. Xu, P. Tang, Structures of highly flexible intracellular domain of human α7 nicotinic acetylcholine receptor, Nat. Commun. 13 (2022) 793, https://doi.org/10.1038/s41467-022-28400-x.
[9] S.J. Moss, B.J. McDonald, Y. Rudhard, R. Schoepfer, Phosphorylation of the predicted major intracellular domains of the rat and chick neuronal nicotinic acetylcholine receptor α7 Subunit by cAMP-dependent protein kinase, Neuropharmacology 35 (1996) 1023–1028, https://doi.org/10.1016/S0028-3908(96)00083-4.
[10] J.R. King, J.C. Nordman, S.P. Bridges, M.-K. Lin, N. Kabbani, Identification and characterization of a G protein-binding cluster in alpha 7 nicotinic acetylcholine receptors, J. Biol. Chem. 290 (2015) 20060–20070, https://doi.org/10.1074/jbc.M115.647040.
[11] S. Shaw, M. Bencherif, M.B. Marrero, Janus kinase 2, an early target of α7 nicotinic acetylcholine receptor-mediated neuroprotection against Aβ-(1–42) amyloid, J. Biol. Chem. 277 (2002) 44920–44924, https://doi.org/10.1074/jbc.M204610200.
[12] A.I. Chernyavsky, I.B. Shchepotin, S.A. Grando, Mechanisms of growth-promoting and tumor-protecting effects of epithelial nicotinic acetylcholine receptors, Int. Immunopharm. 29 (2015) 36–44, https://doi.org/10.1016/j.intimp.2015.05.033.
[13] P. Komal, J. Estakhr, M. Kamran, A. Renda, R. Nashmi, cAMP-dependent protein kinase inhibits α7 nicotinic receptor activity in layer 1 cortical interneurons through activation of D1/D5 dopamine receptors, J. Physiol. 593 (2015) 3513–3532, https://doi.org/10.1113/JP270469.
[14] M.B. Yaffe, K. Rittinger, S. Volinia, P.R. Caron, A. Aitken, H. Leffers, S.J. Gamblin, S.J. Smerdon, L.C. Cantley, The structural basis for 14-3-3:phosphopeptide binding specificity, Cell 91 (1997) 961–971, https://doi.org/10.1016/s0092-8674(00)80487-0.
[15] B. Xiao, S.J. Smerdon, D.H. Jones, G.G. Dodson, Y. Soneji, A. Aitken, S.J. Gamblin, Structure of a 14-3-3 protein and implications for coordination of multiple signalling pathways, Nature 376 (1995) 188–191, https://doi.org/10.1038/376188a0.
[16] G. Gogl, K.V. Tugaeva, P. Eberling, C. Kostmann, G. Trave, N.N. Sluchanko, Hierarchized phosphotarget binding by the seven human 14-3-3 isoforms, Nat. Commun. 12 (2021) 1677, https://doi.org/10.1038/s41467-021-21908-8.
[17] N.N. Sluchanko, D.M. Bustos, Intrinsic disorder associated with 14-3-3 proteins and their partners, Prog Mol Biol Transl Sci 166 (2019) 19–61, https://doi.org/10.1016/bs.pmbts.2019.03.007.
[18] A. Aitken, 14-3-3 proteins: a historic overview, Semin. Cancer Biol. 16 (2006) 162–172, https://doi.org/10.1016/j.semcancer.2006.03.005.
[19] S. Mazzaferro, S.T. Whiteman, C. Alcaino, A. Beyder, S.M. Sine, NACHO and 14-3-3 promote expression of distinct subunit stoichiometries of the alpha 4 beta 2 acetylcholine receptor, Cell. Mol. Life Sci. 78 (2021) 1565–1575, https://doi.org/10.1007/s00018-020-03592-x.
[20] E.M. Jeanclos, L. Lin, M.W. Treuil, J. Rao, M.A. DeCoster, R. Anand, The chaperone protein 14-3-3 eta interacts with the nicotinic acetylcholine receptor alpha 4 subunit - evidence for a dynamic role in subunit stabilization, J. Biol. Chem. 276 (2001) 28281–28290, https://doi.org/10.1074/jbc.M011549200.
[21] M.M. Rosenberg, F. Yang, M. Giovanni, J.L. Mohn, M.K. Temburni, M.H. Jacob, Adenomatous polyposis coli plays a key role, in vivo, in coordinating assembly of the neuronal nicotinic postsynaptic complex, Mol. Cell. Neurosci. 38 (2008) 138–152, https://doi.org/10.1016/j.mcn.2008.02.006.
[22] H. Sun, X. Lin, H. Zhang, Y. Zhang, Z. Liu, A consensus phosphoserine within the large cytoplasmic loop of insect nAChR α8 subunits modulated interaction between 14-3-3ε and nAChRs to regulate neonicotinoid efficacy, Pestic. Biochem. Physiol. 192 (2023), 105384, https://doi.org/10.1016/j.pestbp.2023.105384.
[23] E.N. Lyukmanova, Z.O. Shenkarev, A.A. Schulga, Y.S. Ermolyuk, D. Yu Mordvintsev, Y.N. Utkin, M.A. Shoulepko, R.C. Hogg, D. Bertrand, D. A. Dolgikh, V.I. Tsetlin, M.P. Kirpichnikov, Bacterial expression, NMR, and electrophysiology analysis of chimeric short/long-chain α-neurotoxins acting on neuronal nicotinic receptors, J. Biol. Chem. 282 (2007) 24784–24791, https://doi.org/10.1074/jbc.M611263200.
[24] E.N. Lyukmanova, A.A. Shulga, D.A. Arsenieva, K.A. Pluzhnikov, D.A. Dolgikh, A. S. Arseniev, M.P. Kirpichnikov, A large-scale expression in Escherichia coli of neurotoxin II from Naja oxiana fused with thioredoxin, Russ. J. Bioorg. Chem. 30 (2004) 25–34, https://doi.org/10.1023/B:RUBI.0000015770.38602.e3.
[25] A.A. Kapitonova, K.V. Tugaeva, L.A. Varfolomeeva, K.M. Boyko, R.B. Cooley, N. N. Sluchanko, Structural basis for the recognition by 14-3-3 proteins of a conditional binding site within the oligomerization domain of human nucleophosmin, Biochem. Biophys. Res. Commun. 627 (2022) 176–183, https://doi.org/10.1016/j.bbrc.2022.08.047.
[26] D.S. Kulbatskii, M.A. Shulepko, N.N. Sluchanko, E.O. Yablokov, R.A. Kamyshinsky, Y.M. Chesnokov, M.P. Kirpichnikov, E.N. Lyukmanova, Efficient screening of ligand-receptor complex formation using fluorescence labeling and size-exclusion chromatography, Biochem. Biophys. Res. Commun. 532 (2020) 127–133, https://doi.org/10.1016/j.bbrc.2020.08.021.
[27] A. Vagin, A. Teplyakov, Molecular replacement with MOLREP, Acta Crystallogr D Biol Crystallogr 66 (2010) 22–25, https://doi.org/10.1107/S0907444909042589.
[28] G.N. Murshudov, P. Skubák, A.A. Lebedev, N.S. Pannu, R.A. Steiner, R.A. Nicholls, M.D. Winn, F. Long, A.A. Vagin, REFMAC5 for the refinement of macromolecular crystal structures, Acta Crystallogr D Biol Crystallogr 67 (2011) 355–367, https://doi.org/10.1107/S0907444911001314.
[29] P. Emsley, K. Cowtan, Coot: model-building tools for molecular graphics, Acta Crystallogr D Biol Crystallogr 60 (2004) 2126–2132, https://doi.org/10.1107/S0907444904019158.
[30] N.N. Sluchanko, Recent advances in structural studies of 14-3-3 protein complexes, Adv Protein Chem Struct Biol 130 (2022) 289–324, https://doi.org/10.1016/bs.apcsb.2021.12.004.
[31] I.V. Maslennikov, Z.O. Shenkarev, M.N. Zhmak, V.T. Ivanov, C. Methfessel, V. I. Tsetlin, A.S. Arseniev, NMR spatial structure of alpha-conotoxin ImI reveals a common scaffold in snail and snake toxins recognizing neuronal nicotinic acetylcholine receptors, FEBS Lett. 444 (1999) 275–280, https://doi.org/10.1016/s0014-5793(99)00069-1.
[32] B. Dirnberger, D. Korona, R. Popovic, M.J. Deery, H. Barber, S. Russell, K.S. Lilley, Enrichment of membrane proteins for downstream analysis using styrene maleic acid lipid particles (SMALPs) extraction, Bio Protoc 13 (2023), e4728, https://doi.org/10.21769/BioProtoc.4728.
[33] L.M. Stevers, E. Sijbesma, M. Botta, C. MacKintosh, T. Obsil, I. Landrieu, Y. Cau, A. J. Wilson, A. Karawajczyk, J. Eickhoff, J. Davis, M. Hann, G. O'Mahony, R. G. Doveston, L. Brunsveld, C. Ottmann, Modulators of 14-3-3 protein-protein interactions, J. Med. Chem. 61 (2018) 3755–3778, https://doi.org/10.1021/acs.jmedchem.7b00574.
[34] I. O'Kelly, M.H. Butler, N. Zilberberg, S.A.N. Goldstein, Forward transport. 14-3-3 binding overcomes retention in endoplasmic reticulum by dibasic signals, Cell 111 (2002) 577–588, https://doi.org/10.1016/s0092-8674(02)01040-1.